Characteristics of Volcanic Ash in a Gas Turbine Combustor and Nozzle Guide Vanes

Lei-Yong Jiang
Aerospace, the National Research Council of Canada
1200 Montreal Road, M-10, Ottawa, Ontario, CANADA, K1A 0R6
lei-yong.jiang@nrc-cnrc.gc.ca

Yinghua Han
Aerospace, the National Research Council of Canada
1200 Montreal Road, M-10, Ottawa, Ontario, CANADA, K1A 0R6
yinghua.han@nrc-cnrc.gc.ca

Prakash Patnaik
Aerospace, the National Research Council of Canada
1200 Montreal Road, M-17, Ottawa, Ontario, CANADA, K1A 0R6
prakash.patnaik@nrc-cnrc.gc.ca

ABSTRACT

To understand the physics of volcanic ash impact on gas turbine hot-components and develop much-needed tools for engine design and fleet management, the behaviours of volcanic ash in a gas turbine combustor and nozzle guide vanes (NGV) have been numerically investigated. The study is divided into two steps, one for the combined combustor-NGVs and the other for a single high-fidelity NGV, where the results from the first step are used as the inlet boundary conditions for the second. High-fidelity numerical models are generated, and volcanic ash sample, physical and thermal properties are identified. The current fine particle rebound and deposition models and volcanic ash experimental data are searched, and a simple critical particle viscosity – critical wall temperature model is proposed to account for ash particles bouncing off or sticking on metal walls. A user defined function is written to link this model to a commercial code. To the authors' knowledge, it is the first study on detailed ash behaviours inside practical gas turbine hot-components in open literature, and from this effort, a framework has been built.

The results indicate that due to the particle inertia and combustor geometry, the volcanic ash concentration in the NGV cooling passage increases with ash size, density and inlet velocity in general, and can reach three and half times as high as that at the air inlet for the conditions investigated. The ash capture efficiency at the NGV external walls dramatically increases as the turbine inlet temperature approaches to the metal melting temperature. More importantly, the majority of the ash particles entering the NGV cooling chamber are trapped in the cooling flow passage for all four turbine inlet temperature conditions. This may reveal another volcanic ash damage mechanism originated from engine cooling flow passages, particle trap > geometry and heat transfer change > metal wall temperature increase > ash deposit and metal burn. To intelligently mitigate volcanic ash impact and develop required tools for OEMs and end users, some suggestions are recommended at the end of the paper.

1.0 INTRODUCTION

The world's busy air traffic corridors pass over or downwind of hundreds of volcanoes capable of hazardous

explosive eruptions. When a volcanic eruption occurs, significant ash particulate clouds are formed and drift at different altitudes, for hundreds of kilometers depending on evolving meteorological conditions, which causes a major concern to aviation [1].

Volcanic ash threat, damage mechanisms, and devastating incidents occurred in the last three decades have been described by Dunn [2] and Davison & Rutke [3]. One of the three damage mechanisms is the ash deposition on gas turbine hot components due to so-called glassification. It is believed that as ash particles enter the combustor, they pass through hot combustion regions (~1600-2300 K), get rapidly heated above the transition temperature, then become soft or form a melt, and eventually stick on the walls of the combustor and turbine stages as solid deposits [2-6]. The deposits affect the turbine aerodynamics, and can lead to a loss of power or engine malfunction.

A series of experimental tests on deposition of volcanic materials in the hot-sections of two gas turbine engines, Allison T56 and Pratt and Whitney F-100, at high concentration levels (250 and 500 mg/m^3), were performed in later 1980s and early 1990s [7-11], and summarized by Kim et al [6]. The test rigs were built from real engine components, and were operated at the same flow function and temperature levels as would occur in the operational engines. For the T56 engine tests, Twin Mountain black scoria (volcanic ash) and a blend of Hollywood sand, Corona clay, bentonite and Twin Mountain black scoria were selected as the test materials, with the average particle size from 5 to 73 μm. The turbine inlet temperature varied from 1222 to 1506 K, and the ash capture ratios were obtained. The results indicated: (1) the turbine inlet temperature and vane surface temperature were two dominant parameters for ash deposits; (2) deposition was observed in some cases on the turbine inlet temperature probes and the nozzle guide vanes; (3) the distribution of deposits was strongly influenced by whether or not the particles were able to follow the engine flow path. However, up to now little data was available on engine tests at low to mid concentrations (0.1-10 mg/m^3) [1, 3].

As pointed out by a group of experts on the volcanic ash effects on military aircraft platforms [1], a comprehensive research base does not exist, such as potential volcanic ash effects, post-exposure impact, service-life reduction, etc., and a lack of this knowledge has led to the adoption of the conservative policy of total volcanic ash avoidance. One of the key recommendations from them is to establish computer-based methods to reconcile real-time data and modeling predictions for flight route planning.

In this paper, the characteristics of volcanic ash particles in a can-annular combustor and nozzle guide vanes (NGVs) are numerically investigated. Such knowledge is essential to understand the behaviours or nature of volcanic ash inside engine hot-sections, to develop numerical models for predicting volcanic ash impact and deposition, and to provide needed tools to OEMs in engine design and end-users in fleet management. To the authors' knowledge, this is the first study on the detailed ash behaviours inside practical gas turbine hot-components in open literature.

The investigation is divided into two steps: one for the combined combustor and 10 simplified NGVs, and the other for a single high-fidelity NGV. The results at the corresponding locations from the first step are used as the inlet boundary conditions for the second step. The high-fidelity CFD models, numerical methods, rebound and deposition models, a user defined function for a proposed simple volcanic ash rebound and sticking model, engine operating conditions, boundary conditions, numerical results and findings are described in the following sections. Finally, the paper provides conclusions and recommendations going forward.

2.0 HIGH-FIDELITY CFD MODELS

2.1 Computational Domain and Mesh of Combined Combustor-NGVs

A conventional can-annular gas turbine combustor was chosen for this study. The computational domain includes a combustion can, a 60-degree annular chamber and 10 simplified NGVs. The whole mesh is shown in Fig. 1(a), the zoomed view of three thermocouples in front of NGVs and ten NGV cooling air slots at the downstream end of the annular chamber are illustrated in Fig. 1(b), and the high-fidelity combustion can mesh is illustrated in Fig. 1(c), including the dome swirler, fuel nozzle body, ignitor body, wiggle strips, mixing and dilution holes, baffles and splashing holes, thermocouples, and ten NGVs. For the simplified NGVs, only the external surfaces were meshed, and the internal cooling flow passages and solid bodies were not considered in this piece of work. To compensate the NGV cooling effect, the averaged cooling flux from the simulation of a single high-fidelity NGV [12] was defined at the NGVs external surfaces. More details of the mesh and mesh independent study can be found in [13]. A mesh with 17.4 million cells was used for all the simulations.

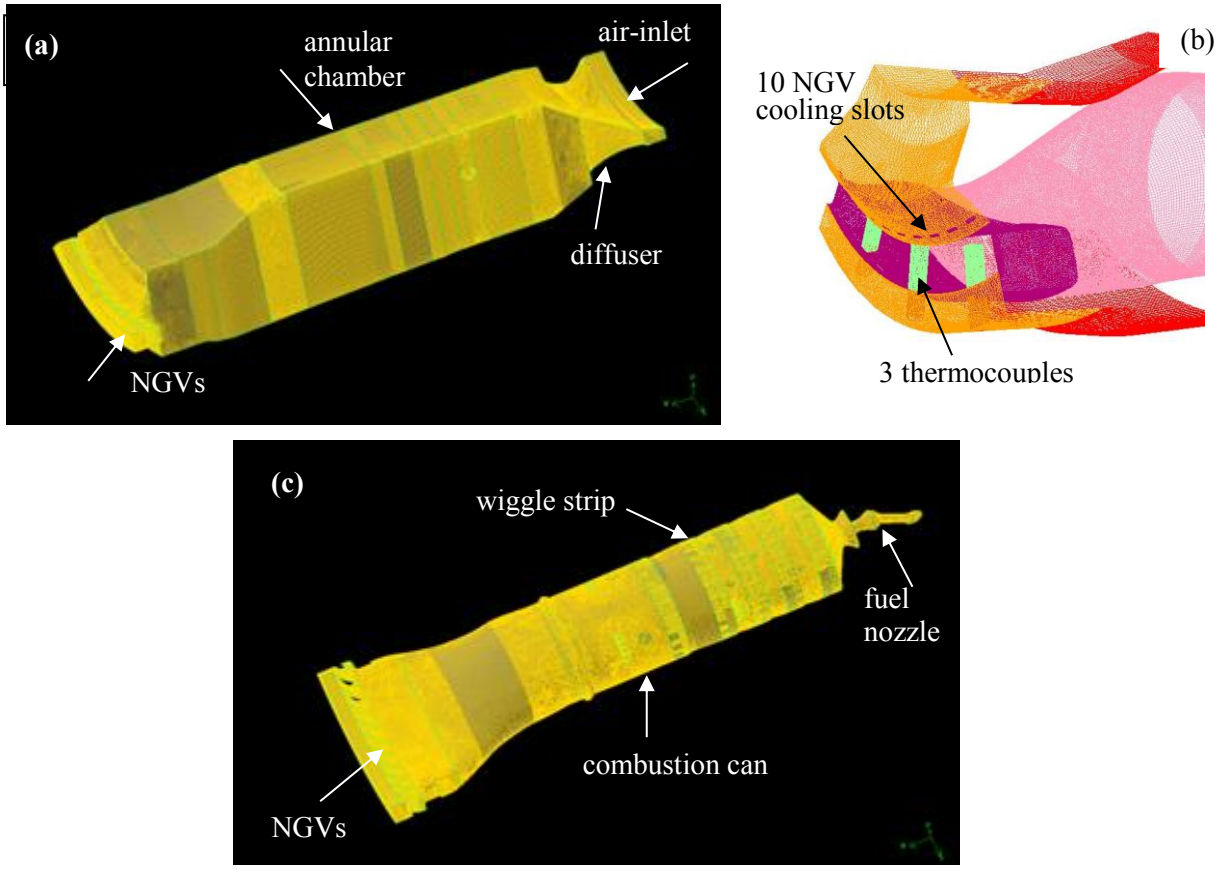

Fig. 1 Computational domain and mesh of a 60-deg sector of the combustor: (a) the whole mesh, (b) the thermocouple and NGV slot mesh, and (c) the can and NGVs mesh

As shown in Fig. 1, compressed air enters the annular chamber through a narrow annulus, and then decelerates through the diffuser before being split among the liner openings. The liquid droplets from the fuel nozzle evaporate, mix and react with the air that enters through the dome swirler, primary holes and wiggle strips. The hot gas mixture continues to burn with the air from the secondary holes and wiggle strips, cools further downstream by the air from the dilution holes, and eventually reaches NGVs. Note that a small

amount of the compressed air flows out of the domain through ten NGV cooling slots. Concurrently, volcanic particles enter the combustor through the annular air inlet, and travel with air through all flow passages in the domain, and various behaviours such as dynamic delay, heating up, cooling down, softening, melting, impinging, rebounding or sticking on metal surfaces may occur.

2.2 Computational Domain and Mesh of Single NGV

For the second step, the single NGV meshes for the whole domain and metal regions are illustrated in Fig. 2 (a) and (b) respectively. It is a 6-degree sector in the whole combustor coordinates. The computational domain begins upstream of the flat plates of the internal and external shrouds, and is extended to half of the NGV chord length in the downstream direction. Fine nodes were laid near the NGV internal and external walls, cooling air slot, holes, and fins in order to properly solve conjugate heat transfers; while coarse nodes were used in the flow regions which were away from the NGV walls. Finally, a mesh with 15.9 million cells was used for all simulations. More details of the mesh and y+ value consideration can be found in [12].

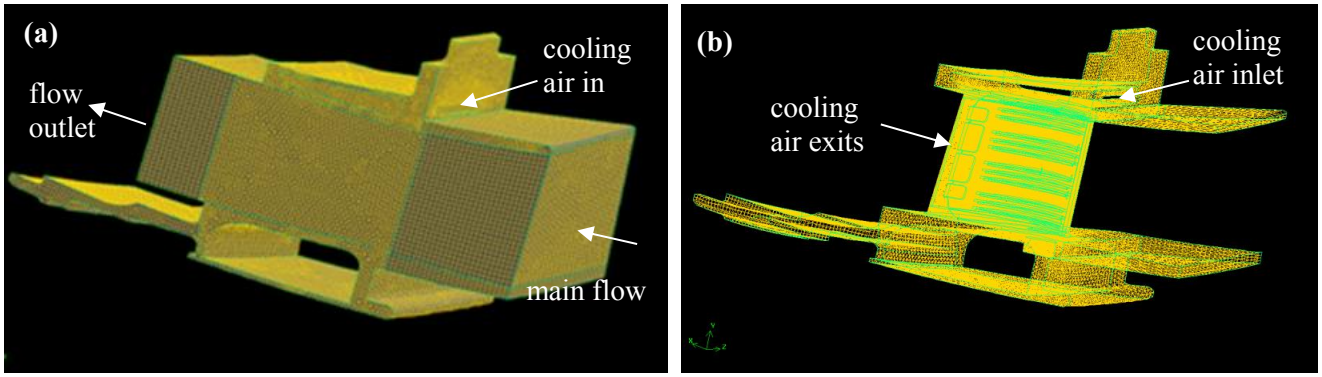

Fig. 2 NGV domain and meshes: (a) the whole mesh, and (b) the mesh in metal regions

As shown in Fig. 2, the main flow, hot gas mixture and ash particles, from the combustor flows over the NGV body; while the cooling air and ash particles from the combustor annular chamber enter the NGV cooling chamber through the air inlet above the flat plate of the internal shroud, pass through the cooling slot, holes and fins, exit at the four rectangular exits, then merge with the main flow, and flow out of the flow domain. Through impingement and convection, the cooling air absorbs heat from the NGV walls and lowers their surface temperature. In these processes, the behaviours of volcanic ash particles inside and outside of the cooling chamber can be observed.

3.0 NUMERICAL METHODS

3.1 Eulerian-Lagrangian Approach for Dilute Discrete Droplets and Particles in Fluid-Field

The traditional Eulerian-Lagrangian approach was used to solve the multiphase, steady, turbulent, compressible, reacting or non-reacting flows in the present work [14-15]. Three phases, solid particles, liquid fuel droplets and gaseous mixture, were considered for the combined combustor-NGVs simulations, and two phases, solid particles and gaseous mixture, were resolved in the single NGV simulations. For both cases, the volume fraction of droplets and ash particles was negligibly small, 6.7×10^{-5} to 1.7×10^{-4} for fuel droplets and 1.4×10^{-6} for ash particles, and therefore the discrete Lagrangian particle tracking method was an ideal approach without compromising the numerical solutions [14-15]. The gaseous mixture was treated as a continuum, and the Favre-averaged conservation equations for mass, momentum, species and total enthalpy

were resolved. For the discrete phases, a large number of droplets or particles were tracked through the calculated gaseous flow domain, and each trajectory was predicted by balancing the flow induced forces on the droplet or particle with its inertia along its path. Exchanges of mass, momentum, species and energy between the gas mixture and fuel droplets were computed accordingly in the combined combustor-NGVs simulations. For both steps, the effect of ash particles on the flow was neglected due to the negligible volume fraction of particles.

For closure of the flow conservation equations, the turbulence transfer terms and sources had to be properly treated. For the combined combustor-NGVs simulations, the realizable k-ε model was selected for turbulence transfers, and the eddy dissipation (EDS) combustion model was used to account for species source terms [12]. For the single NGV case, the turbulence transfers were modeled by the SST k-ω model (the shear-stress transport-model) [16]. For the conjugate or coupled heat transfer between the metal and flow fields, both fluid and solid regions were solved together.

3.2 Rebound and Deposition Modelling of Volcanic Ash Particles at Metal Surfaces

One key issue for reliable prediction of volcanic ash particles passing through the combustor and NGVs is to understand and adequately model the rebound and deposition behaviours as they impinge on metal walls. A number of numerical models have been proposed with limited success. Starting from governing equations, two rebound models of spherical micro-particles were developed by Jim & Dunn [17]. The first one considered the effects of surface roughness and Hertzian and adhesion damping, and the second included both elastic and plastic deformations. The model constants were calibrated against a number of experimental datasets for different materials. Most of the experiments were carried out at low velocities (< 25 m/s), impingement angle of 90 degrees, and particle size less than 10.0 μm.

Fine particle rebound studies relevant to gas turbine engine conditions are rare. Recently, the rebound restitution coefficients of Arizona road dust particles impinging on polished 304 stainless steel coupons at three high temperatures (533, 866 and 1073 K) were reported by Reagle et al [18]. The experiments were carried out at different velocities and impingement angles, and the particle nominal size was in a range of 20 – 40 μm. They pointed out that as the temperature increased the reduction in elastic modulus and yield strength of the steel along with the material changes of the dust particles was expected to play an important role in the impact mechanics. It was also realized that temperatures up to 1073 K did not significantly reduce the restitution coefficients.

Numerical studies were conducted by Ai & Fletcher [19] to simulate coal ash (mean diameter of 16 μm) deposition around film cooling holes of test coupons for gas turbine vanes at M = 0.25 and T = 1293-1453 K. In their work, the deposition model from El-Batsh & Haselbacher [20] was used, which was based on the earlier work of Brach & Dunn [21] and Soltani & Ahmadi [22]. The model consisted of two processes: the sticking process, a pure mechanical interaction in the absence of the fluid force, and the detachment process, a fluid dynamic interaction between the fluid and adhered particles. For the first process, a capture or critical velocity is defined as

$$u_{cr} = \left[(2E)/d_p\right] \tag{1}$$

where E is the Young's modulus and d_p is the particle diameter. It says that if the particle normal impact velocity is smaller than the critical velocity, the particle sticks; otherwise, the particle bounces back. To apply this sticking model in their prediction, the dependency of Young's modulus on temperature was tuned to match the capture efficiency obtained in the experiments.

For the second process, a critical wall shear velocity is given by the following equation

$$v_{sh}^2 = \frac{C_u W_A}{\rho d_p}\left(\frac{W_A}{d_p K_c}\right)^{1/3} \tag{2}$$

where v_{sh} is the shear velocity, Cu stands for the Cunningham correction factor, W_A denotes the stick force, ρ is density, and K_c represents composite Young's modulus. The relevant parameters and more details regarding the interaction between the particle and wall are given in [20]. The model means that the particle will be removed from the surface if the local wall shear velocity in the turbulent flow is larger than the critical shear velocity.

Barker et al [23] numerically modeled coal ash (d ≤ 40 μm) deposition on a GE-E^3 high pressure turbine vane passage. The above critical velocity model was improved by using the composite Young's modulus to account for particle and metal surface interaction, that is

$$E = 0.51\left[\frac{5\pi^2\left[\left(1-\nu_S^2\right)/\pi E_S + \left(1-\nu_P^2\right)/\pi E_P\right]}{4\rho P^{3/4}}\right] \tag{3}$$

where υ is the Poisson ratio, and subscripts p and s stand for the particle and metal surface respectively. In addition to the critical velocity model, a critical viscosity sticking model was used for deposition prediction. The critical viscosity model was developed by Tafti and Sreedharan [24], based on the particle viscosity variation with temperature. The probability of particle sticking is determined by the following expression

$$\mathrm{Prob}\left(P_{st}\right) = \frac{\mu_{cr}}{\mu_{T_P}} \tag{4}$$

In Eq. (4), μ_{cr} is the particle critical viscosity at the critical or softening temperature, and μ_{Tp} represents the viscosity of the particle at the current temperature. That is, if the particle viscosity is equal or less than the critical viscosity, the particle sticking occurs or the sticking probability is 100%; otherwise the sticking probability is calculated from Eq. (4). It was found that both numerical models were able to predict the trends of deposition, particularly for the initial stage; however both models had fundamental weaknesses that had to be resolved in the future.

The effect of slot film cooling on sub-bituminous ash deposition in a high pressure nozzle guide vane flow passage was studied by Prenter et al [25], where the critical viscosity sticking model was also used. To improve deposition prediction, the relationship between the particle temperature and its viscosity was adjusted based on experimental results [25-26], and the particle critical temperature was raised from 1422 to 1997 K. In addition, it was suggested that the metal surface temperature and local shear stress should be considered in the sticking model.

The above models and experimental data may represent the current state-of-the-art for fine particles impinging on metal surfaces. Owing to the rich parameter space (flow dynamics, heat transfer, softening, melting, solidification, elastic/plastic deformation, material properties, surface roughness, etc.) and harsh operating conditions, the model development and experimental study on volcanic ash ingestion in the engine hot section are challenging. With intelligent planning and collaboration, the dominating parameters can be identified, the required experimental tests can be cost-effectively carried out, and this issue can be solved to meet engineering requirements.

Due to the lack of experimental data relevant to gas turbines, based on the above critical viscosity model, a simple critical particle viscosity - critical wall temperature model is proposed in the present work to account for volcanic particle rebound and deposit at metal walls, that is

$$\Pr ob\left(P_{st}\right)=\left\{\min\left[\frac{\mu_{cr}}{\mu_{T_P}},\,1.0\right]\right\}^{C_A}\times\left\{\min\left[\frac{T_{T_w}}{T_{cr}},\,1.0\right]\right\}^{C_B} \tag{5}$$

where T_w is the local wall temperature, T_{cr} is the metal critical or melt temperature, and C_A and C_B are constants, and a reduction number of 2.0 is used for the time being. Note that in Eq. (5), instead of the softening viscosity, the particle melt viscosity is defined as the critical viscosity and at or lower than this viscosity the particle is melted and shows "flow" behaviour [5, 27].

In this model, the most important parameters in the event of particle rebound and sticking processes [6-11] are considered to be the particle viscosity and metal wall temperature. The probability of particle sticking on metal walls is determined by the ratio of the particle critical viscosity to current viscosity and the ratio of the current wall temperature to material melt temperature. This makes the model more reasonable, that is, as the particle temperature is equal to or higher than the particle melt temperature and the local wall temperature is equal to or greater than the metal melt temperature, the "flow" particle will stick on the "melting" wall with a 100% probability. Based on the S_iO_2 content of the volcanic ash considered in this work (please see the sub-section 3.3), the particle viscosity at 1770 K was specified as the critical viscosity, and the metal melt temperature (Hastelloy X) of 1600 K was defined as the critical wall temperature.

For the particle viscosity higher than the critical viscosity or the local wall temperature below the critical material temperature, the particle sticking probability is less than 100%, i.e., some particles will bounce back from the wall and some will stick on the wall. In order to implement this formulation, a uniform random number generator was used to generate a random number in the range of 0 to 1 for each particle impact. If the random number was less than the calculated sticking probability, the particle would deposit on the wall; otherwise the particle would bounce back from the wall. As an example, the particle softening temperature was close to 1200 K for the present work [5], and the corresponding probability was only $1.3\text{x}10^{-4}$ for the local wall temperature of 1200 K. As a result, the particle would most likely bounce back from the wall.

For particles bouncing back from the wall, the restitution coefficients of Arizona road dust particles on 304 stainless steel coupons measured by Reagle et al [18] were used to model the particle rebound behaviour since the experimental temperature range was relatively high, the particle chemical composition was similar to the volcanic ash used in the present study, and the particle sizes were close to the middle range of those used in the present study (please see the sub-section 3.3).

To implement the above ideas and related parameters, a user-defined-function was written, complied, and linked to a commercial CFD code, FLUENT, and verified step by step to account for ash particle rebound and deposit at metal walls.

3.3 Thermo-Physical Properties of Volcanic Ash

To simulate the behaviour of volcanic ash passing through the engine hot-section, it is essential to have a good knowledge of ash thermo-physical properties. Unfortunately the detailed investigation of these properties is scarce. In this paper, the viscosity (T = 1373–1598 K), thermal conductivity (T = 293–1623 K), and specific heat (T = 347–1671 K) of the Pietre-Cotte lava, Vulcano, Italy from Ebert et al [27] were used. Due to the narrow temperature range for viscosity, the volcanic ash viscosity versus temperature relationship (T = 873-

1873 K) for the Redoubt volcano, Alaska was supplemented, which was calculated by Mastin [28] using a model developed by Giordano et al [29]. Note that the main compositions, S_iO_2 and Al_2O_3, from the Pietre-Cotte lava and Redoubt volcano, were close to each other, i.e., 73.4%, 13.4% and 73.6%, 14%, respectively. Outside of the valid temperature ranges, extrapolation was used to estimate the required thermos-physical properties.

The melting or sticking temperature is one of the most important parameters to assess volcanic ash deposition in the engine. The melting evolution of nine volcanic ashes around the world for S_iO_2 content from 50% to 71% was systematically investigated by Song et al [5], and four characteristic temperatures were defined: shrinkage, deformation, hemispherical, and flow. It was found the shrinkage temperature of these nine samples varied from ~1200–1420 K, while the "flow" temperature was in a range of ~1540–1770 K. For the sample with 71.4% S_iO_2 content, the shrinkage and flow temperatures were 1200 K and 1770 K, and the latter was used in the proposed particle rebound and sticking model.

During volcanic eruptions, large particles fall rapidly and small ash particles (<200 μm at reduced concentrations) have a long atmospheric residence time and can be transported great distances [3, 30]. The volcanic ash size distribution used in this paper is shown in Fig. 3, grouped into five bins with a density of 1440 kg/m^3. These data were measured by De Giorgi et al [31] for the Etna volcano ash sample. Note that the density of volcanic ash could vary significantly from ~700 to 3300 kg/m^3 [32], and the value of 1440 kg/m^3 was used for most of the simulations.

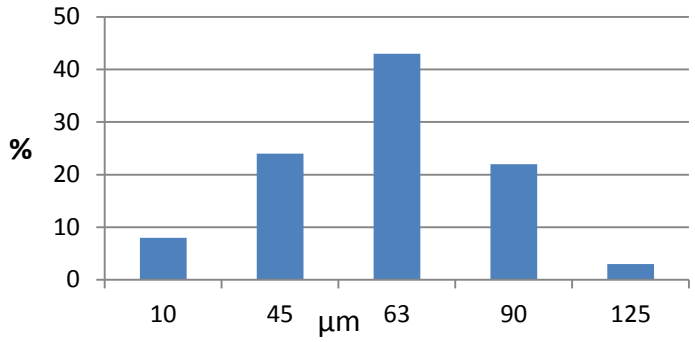

Fig. 3 Volcanic ash size distribution in weight [31]

The volcanic ash particle trajectory is strongly influenced by the particle shape. To account for the non-spherical effect, a particle shape factor is commonly defined as the ratio of the surface area of a sphere that has the same volume as the given particle to the surface area of the particle, that is

$$\phi = \frac{A_{sph\_V}}{A_p} \tag{5}$$

In this paper, a value of 0.68 was used, that was obtained by De Giorgi et al [31] by analysing the Etna volcano ash particles with a scanning electron microscopy. This value was in the range of 0.6–0.8 recommended by Riley et al [30] for three volcanic ash samples. Please note that the drag forces on spherical fuel droplets and non-spherical volcanic particles were calculated with different semi-empirical equations [15].

3.4 Boundary Conditions

Three flight conditions, takeoff, maximum cruise and cruise, provided by Oechsle et al [33] were considered in the present study. For the combined combustor-NGVs case, the combustor inlet airflow rate, fuel flowrate, pressure and temperature, were used as boundary conditions. An estimated turbulence intensity of 5% and the hydraulic diameter of the inlet annulus were used to estimate the turbulent kinetic energy and dissipation rate at the air inlet. Periodic boundaries were defined at the side surfaces of the 60-degree sector.

For fuel spray, the size and velocity of fuel droplets along the nozzle radial direction were from the experimental data measured at the National Research Council of Canada's High-Pressure Spray Facility using a phase Doppler particle analyzer [34]. The fuel flux distributions along the nozzle radial direction wee from Rizk et al [35], where a mechanical patternator was used in a high-pressure rig at Purdue University, Indiana. Fourteen spray cones with 1800 droplets each were specified, giving a total of 25,200 fuel droplets.

For the volcanic ash concentration, a level of 2.0 mg/m^3 was defined, which was considered as a safe boundary by Clarkson [36] and within the range interested by a multi-partnership program reported by Lekki et al [37]. The volcanic ash mass distribution was assumed uniform at the combustor inlet, and that ash particles had the same inlet velocity as the inlet air. The number of particles per volcanic ash size depicted in Fig. 3 was 2,328, and a total of 11,640 particles were tracked for the five sizes.

For the single NGV case, as mentioned earlier, the inlet boundary conditions were obtained from the combined combustor-NGVs simulations. The average total pressure and temperature at the combustor exit and ten NGV cooling slots (Fig. 1) were used at the main and cooling flow inlets (Fig. 2), where the mass flow rates of both flows were maintained by slightly adjusting the inlet total pressures if necessary. The cooling flowrate was 2.3% of the total inlet airflow for cruise and maximum cruise, and 2.5% for takeoff. A turbulence intensity of 10% and hydraulic diameters were used to estimate turbulence kinetic energy and specific dissipation rate at the inlets.

As mentioned in the Introduction, the obtained ash concentrations at the combustor exit and NGV cooling slots from the first step were specified at the main and cooling flow inlets respectively. The number of particles tracked was 28,900 for the main flow and 1500 for the cooling passage. Periodic boundaries were defined at the side surfaces of the 6-degree sector, and a radial equilibrium pressure distribution was ensured at the domain exit to account for the effect of flow tangential velocity on the exit pressure distribution.

3.5 Solution Methods

A segregated solver with a second-order accuracy scheme was used for the combined combustor-NGVs simulations and a coupled solver with a second-order accuracy scheme was selected for the single NGV case. All solutions were well-converged, and the monitored flow parameters at the critical locations remained unchanged for the first four digits. A multiple-node LINUX cluster with 64-bit, 2.6 GHz, and 64 GB RAM per node was used to carry out all simulations. For all materials, polynomials as a function of temperature were used to calculate the required thermal properties.

4.0 RESULTS AND DISCUSSION

For each of the three flight conditions, a large amount of information are available, such as flow features in the combustor and NGV, evaporation, mixing and burn of fuel droplets, trajectory, impingement, rebound and deposition of volcanic particles, effects of particle size, temperature, velocity on rebound and deposition, etc.

In the interests of brevity, only some examples regarding the volcanic ash behaviours in the combustor and NGV at the max-cruise conditions are presented and discussed here. The complex features of the flow fields and conjugate heat transfers can be found in [12-13].

4.1 Results of Combined Combustor-NGVs Simulations

4.1.1 Volcanic Ash Particle Trajectories

Some of the volcanic ash trajectories for particle size of 63 μm are shown in Fig. 4, where the particle path-lines are colored by particle temperature normalized by a typical maximum temperature, T_{max}. The complete trajectories from the combustor air inlet to the downstream exits are shown Fig. 4(a), superimposed by the combustor and NGV sketches. In Fig. 4(b), the trajectory segments in the annular chamber can be observed by blocking the trajectory segments inside the combustion can. As expected, the particle temperature in the annular chamber is low, only ~550 K. For the particles entering the combustion can, the temperature gradually increases and varies downstream, depending on local flow conditions. The particles with high temperature tend to stick on high-temperature metal surfaces of the thermocouples, combustor liner, and NGVs. In general, the volcanic particles that enter the combustor have four destinations: flowing out the domain through the NGV section, passing through the NGV cooling slots (Fig. 1), sticking on the metal surfaces, and trapped in the downstream end of the annular chamber, or sharp slots of baffles and wiggle strips, etc.

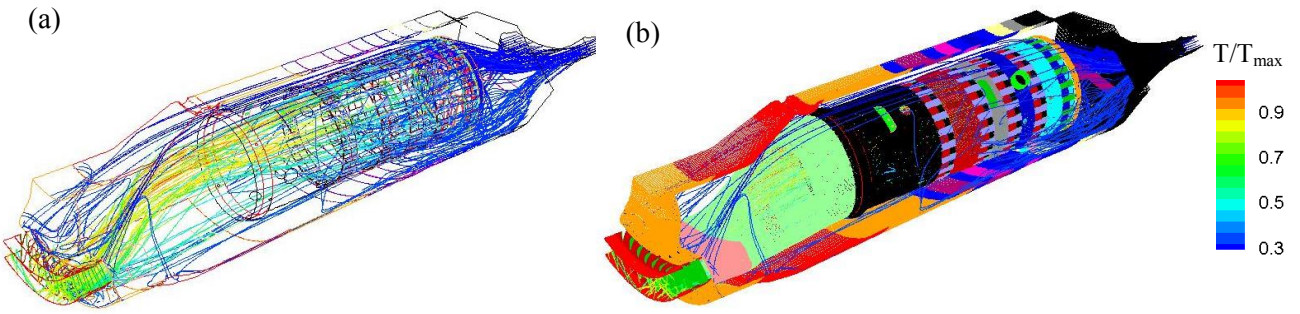

Fig. 4 Volcanic ash particle trajectories for particle size of 63 μm

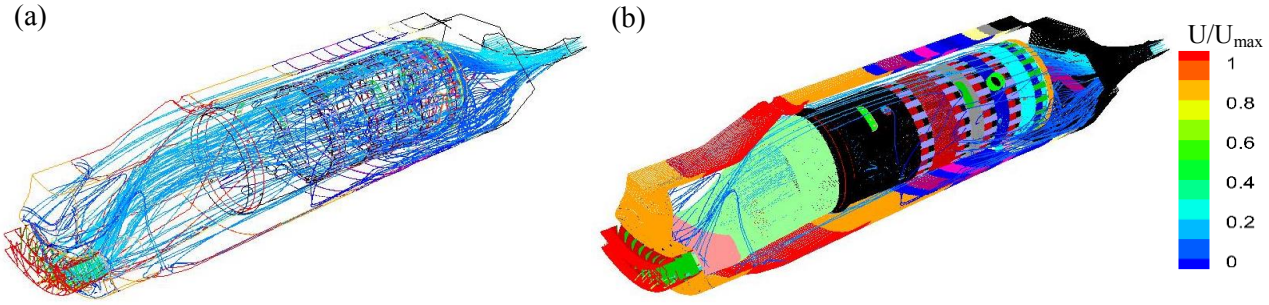

Fig. 5 Volcanic ash particle trajectories for particle size of 63 μm

The same particle trajectories shown in Fig. 4 are shown in Fig. 5, the only difference being colored with the particle velocity magnitude normalized by a typical maximum velocity, U_{max}. The particles enter the annular inlet at relatively high velocity, and decelerate in the diffuser and annular chamber. Most of them enter the combustion can, gradually speed up along their path-lines, and quickly accelerate near the NGV section and exit.

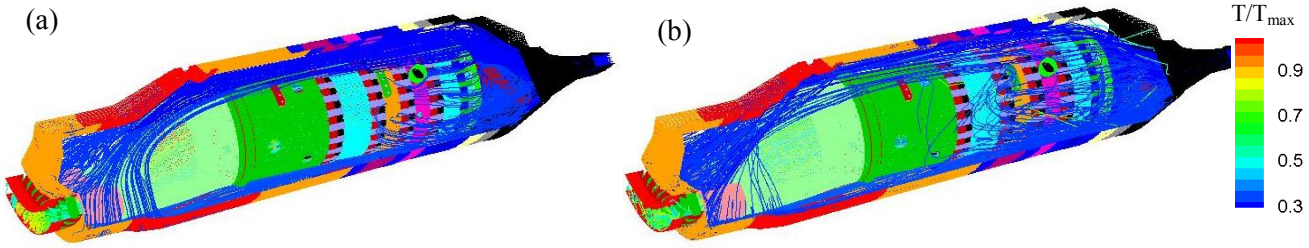

Fig. 6 Volcanic ash particle trajectories: (a) for the particle size of 10 μm, and (b) for the particle size of 125 μm

Figure 6(a) and (b) show some trajectories for the particle size of 10 and 125 μm, respectively. Due to the inertia of particles and sudden 90-deg direction change requirement at the primary, secondary and dilution holes, most particles travel straight forward, impact on the downstream wall of the annular chamber, then bounce back, and eventually enter the can. The tendency to stay in the annular chamber could cause the particle concentration in the NGV cooling slots to be considerably higher than at the inlet concentration.

Moreover, as shown in Fig. 6(a) and (b), a small percentage of particles can enter the combustion can directly from the inlet. Because of the difference in inertia, the 10 μm particles enter the can earlier (through one third upstream portion) than the 125 μm particles (through the half upstream portion). This once again illustrates the effect of particle inertia on particle trajectories.

4.1.2 Effects of Particle Size, Density, and Inlet Velocity on Particle Concentration at the Combustor Exit and in the NGV Cooling Slots

To check the effect of particle dynamic response on the concentration distribution inside the combustor, the particle trajectories for various sizes, inlet velocity, and density were examined individually. Figure 7 shows variations of the volcanic ash concentration, C1, at the combustor exit, and, C2, in the NGV cooling slots with particle size. The concentration here is defined as the volcanic ash mass per unit mass of air, and normalized by the volcanic ash concentration, C0, at the inlet. It can be seen that for all particle sizes, the ash concentration is higher (> 1.0) in the NGV cooling slots, and lower (< 1.0) at the combustor exit than the inlet concentration. In general, the difference between the two curves increases with particle size. This fact indicates that this type of NGV cooling air supply is not preferred.

In Fig. 7, the concentration of C2/C0 is not monotonically increasing with particle size, and a large jump is observed at the size of 63 μm. This may imply that in addition to the particle inertia, the flow-field also has a substantial effect on concentration redistribution. The combustor flow-field is extremely complicated, dominated by a great number of large and small vortices with high turbulence, steep temperature gradients, etc. [12, 34], which certainly affect particle path-lines in the combustor.

The normalized volcanic ash concentrations at the combustor exit and in the NGV cooling slots are displayed in Fig.8, for a particle density range from 700 to 3300 kg/m^3 [32]. For these results, all five particle groups depicted in Fig. 3 are considered together. The particle density has a significant effect on the concentration in

the NGV cooling flow for the density from 2100 to 3300 kg/m^3, and the concentration in the cooling flow is about 3.5 times as high as that in the air inlet at the density of 3300 kg/m^3.

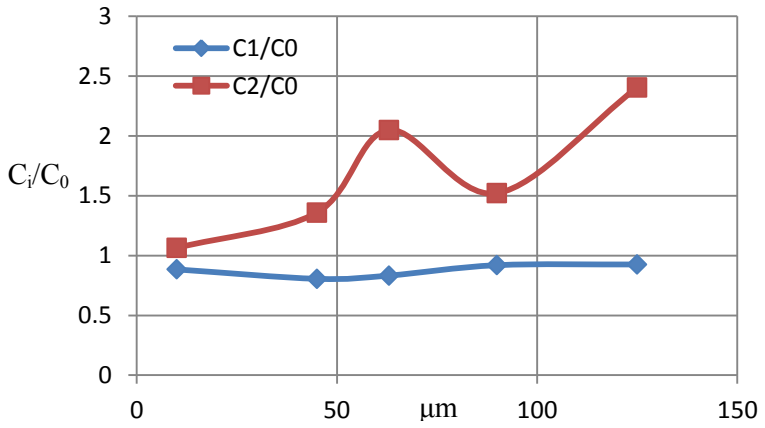

Fig. 7 Volcanic ash concentration variation with particle size

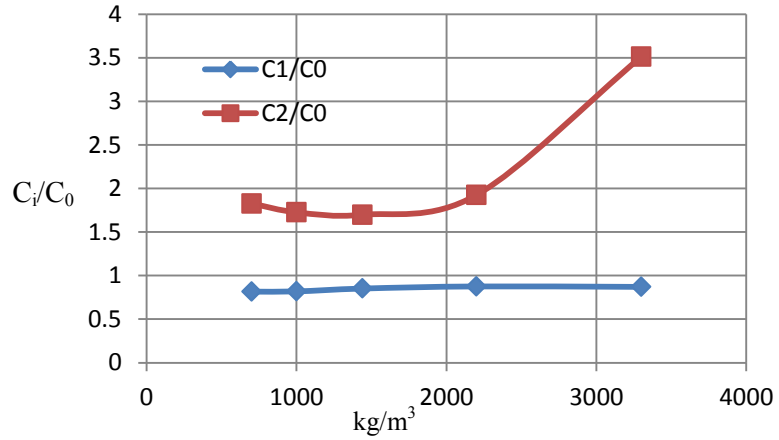

Fig. 8 Volcanic ash concentration variation with particle density

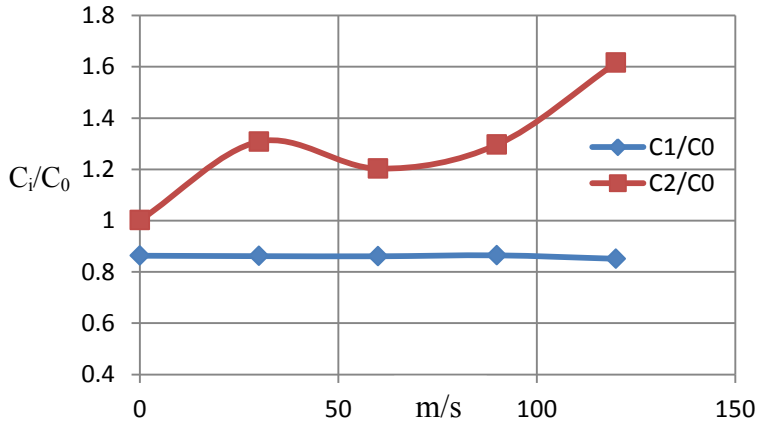

Fig. 9 Volcanic ash concentration variation with particle inlet velocity

The effect of volcanic ash inlet velocity on the normalized concentration at the combustor exit and in the

NGV cooling slots are given in Fig. 9, where the particle inlet velocity varies from 0 to 120 m/s and also the five groups of particles are considered together. Again it can be seen that the concentration is higher in the cooling flow and lower at the combustor exit in comparison with that in the air inlet. The concentration in the NGV slots generally increases with the particle inlet velocity. As shown in Figs. 7-9, the effects of particle size, density and inlet velocity on the ash concentration at the combustor exit is minor since the air flowrate through the cooling slots is only 2.3% of the total inlet air.

4.1.3 Volcanic Ash Capture Efficiency

Figure 10 shows the variation of volcanic ash capture efficiency with the ash particle size, defined as the mass ratio of the ash sticking on metal surfaces over the total inlet ash. Since the ash sticking on the NGV surfaces will be examined in the sub-session 4.2, the deposit on NGV surfaces is not considered in the figure by applying the rebound condition only at the metal surfaces of the NGV section. The capture efficiency varies from 1% to 16%, and has a peak at 45 μm. It is thought that the particles of this size are more likely to be heated to high temperature and impinge on high temperature walls. It should be mentioned that since the proposed simple sticking model in Eq. (5) is not validated against experimental data, the capture efficiency values are only for reference in variation trend studies or volcanic ash characteristics in the combustor and NGVs.

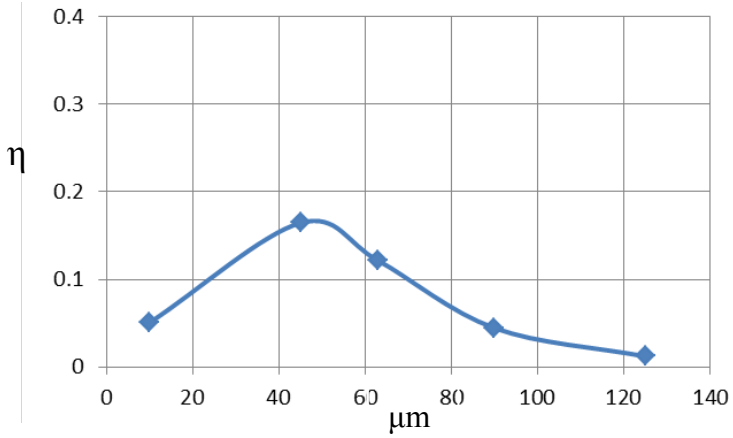

Fig. 10 Volcanic ash capture efficiency in the combustor

The percentage split of the volcanic ash after entering the combustor is given in Table 1. About 10.6% of the particles are captured by the liner walls, 0.4% are trapped in the combustor (most are small particles), and the remainder, 85.2% and 3.8%, feed the NGV main flow and cooling flow respectively, for the single NGV simulations. Please note that although the ash ratio in the combustor versus the NGV cooling slots is 22.4, the corresponding air flow ratio is 42.5. That is, the ash concentration in the NGV cooling flow is nearly twice as high as that at the combustor exit.

Table 1 Volcanic ash splitting

combustor exit	NGV cooling slots	deposit on walls	trapped
85.2 %	3.8 %	10.6 %	0.4 %

4.2 Results of Single NGV Simulations

4.2.1 Volcanic Ash Particle Trajectories

A number of particle trajectories for the NGV main flow and internal cooling flow are illustrated in Fig. 11(a) and (b) respectively, where the NGV and cooling chamber schematics are displayed and the particle path-lines are colored by normalized velocity magnitude. As shown in Fig. 11(a), the particles enter the main flow region at high-speed, slow down near the NGV walls, and accelerate to about sonic velocity at the exit section. In the cooling flow passage, the particle velocities remain low in the cooling chamber, and rapidly speed up and merge with the main flow after exiting the four rectangular outlets.

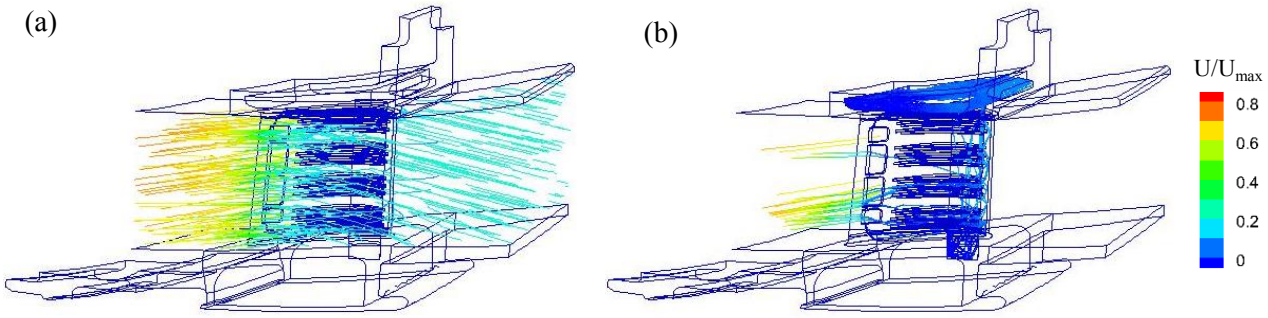

Fig. 11 Volcanic ash particle trajectories: (a) for the main flow, and (b) for the internal cooling flow

Figure 12 shows the same trajectory plots as in Fig. 11, but the particle path-lines are coloured by their normalized temperature. The particle temperature remains high in the main flow, and decreases a little downstream due to acceleration. In the cooling flow, the particle temperature is low in the chamber, ~550 – ~750 K, and quickly increases after leaving the cooling passage.

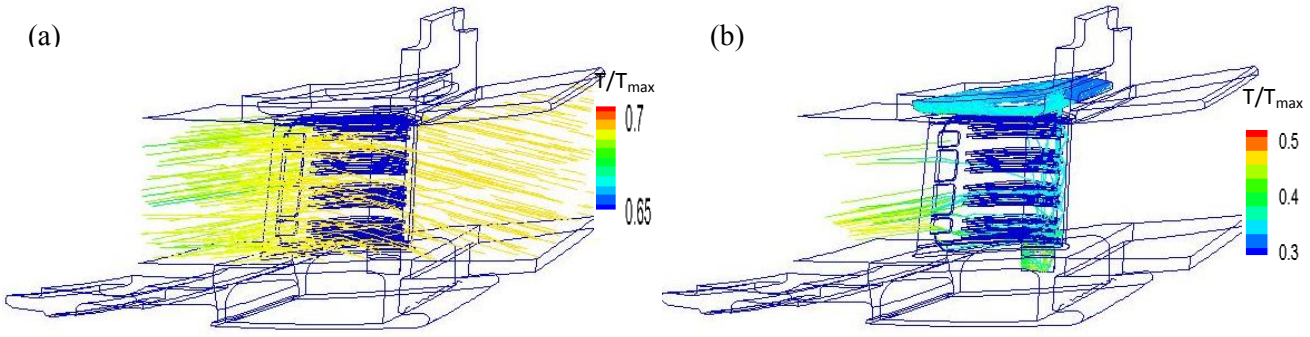

Fig. 12 Volcanic ash particle trajectories: (a) for the main flow, and (b) for the internal cooling flow

More importantly, there is a big difference between the particle trajectories in the main flow and cooling flow. In Fig. 11(a) or Fig. 12(a), most of the particles entering the domain flow out of the domain, and only a small amount may deposit on the metal surfaces. However, in Fig. 11(b) or Fig. 12(b), a large number of the particles are trapped in the internal cooling chamber, and a small portion flow out of the chamber. For the particles passing through the chamber, the average flow time is only ~0.2 second; while for the trapped

particles, even as the flow time increases to hundreds of seconds, the particles still stay in the chamber.

4.2.2 Volcanic Ash Splitting and Capture Efficiency

Since the temperature distribution at the exit of this high life test combustor was not uniform, the single NGV simulations were further carried out with four NGV inlet temperatures, averaged over the four equal areas of the combustor exit. The volcanic ash splitting and capture efficiency results are listed in Table 2 and 3 for the main and internal cooling flow, respectively. The percentage values were calculated based on the ash flowrate at the NGV main inlet for Table 2, and the ash flowrate at the cooling flow inlet for Table 3.

Table 2 Volcanic ash splitting and capture efficiency in the NGV main flow

Cases	inlet gas T^*/T_{max}	deposit	flow out	Trapped
case-1	0.81	28.5%	71.5%	0.0%
case-2	0.72	0.4%	99.6%	0.0%
case-3	0.66	0.0%	100%	0.0%
case-4	0.58	0.0%	100%	0.0%

Table 3 Volcanic ash splitting and capture efficiency in the NGV internal cooling flow

Cases	inlet gas T^*/T_{max}	deposit	flow out	Trapped
case-1	0.81	0.1%	34.7%	65.3%
case-2	0.72	0.0%	31.7%	68.3%
case-3	0.66	0.0%	32.4%	67.6%
case-4	0.58	0.0%	33.3%	66.7%

Two important phenomena are revealed in Table 2 and 3. First, as shown in Table 2, the capture efficiency at the NGV external surfaces is close to 30% for the normalized inlet total temperature of 0.81 (slightly higher than the metal melt temperature), while for the remaining three cases, the capture efficiency is noticeably lower. This fact may suggest that the relationship between the capture efficiency and turbine inlet temperature tends to exponentially increase when the temperature is close to the metal melting point. Furthermore, this fact may imply that if the cooling flow works as designed, the ash deposit on the NGV surfaces would be negligibly small for case-2 to case-4.

The second important observation is that the majority (~65%) of the ash particles entering the cooling chamber are trapped in the cooling passage for all four cases. These trapped particles can build up over the surfaces of cooling fins, holes, narrow slots, etc., block the miniature cooling flow passages, and significantly reduce the cooling capability. As a result, the NGV wall temperature can increase up to the incoming gas stagnation temperature or above the material melting point. Consequently, more ash particles will stick on the NGV external walls. This may reveal another volcanic ash damage mechanism originated in engine cooling flow passages, particle trap > build up > geometry change > flow field and heat transfer change > metal wall temperature rise > ash deposit and metal burn. This mechanism is different from the deposit process described at the beginning, and recognized by Kim et al in the Pratt and Whitney F-100 hot-section testing [6], where the showerhead film cooling holes were blocked and resulted in severe damage to vanes due to the

loss of cooling capability.

These observations suggest that the cooling flow passage blocking can result in serious consequences as the aircraft fly over volcanic ash clouds, and a systematic study of the engine air flow path-lines including the secondary air flow passages should be carried out in order to adequately assess potential volcanic ash damage.

5.0 CONCLUSION AND SUGGESTIONS

A framework to investigate volcanic ash in gas turbine hot components has been built, and successfully applied to a gas turbine engine combustor and NGVs to understand the physics and behaviours of volcanic ash inside engine hot components. It provides the first step to develop much-needed tools for design engineers and end users to mitigate the volcanic ash impact.

The framework is divided into two steps. The results from the combined combustor-NGVs simulations are used as the inlet boundary conditions for the detailed single NGV simulations. To adequately carry out the required tasks, the high-fidelity meshes are generated for both the combined combustor-NGVs and single NGV cases, the volcanic ash sample, physical and thermal properties are identified and specified, the physical numerical models are selected based on the previous benchmark validations, the current fine particle rebound and deposition models and experimental data are searched, a simple critical particle viscosity – wall temperature model for ash particles rebound and deposit on metal surfaces is proposed, and a user defined function is written, verified, and linked to the commercial code. To the authors' knowledge, it is the first study on the detailed ash behaviours inside practical gas turbine hot sections.

The results indicate that local volcanic ash concentration can vary dramatically depending on the geometry and flow path arrangement. Due to the particle inertia and combustor geometry, the volcanic ash concentration in the NGV cooling passage increases in general with ash size, density and inlet velocity, and can be three and half times as high as that in the air inlet. Noticeably, the turbine inlet temperature shows an exponential effect on the ash capture efficiency at the external NGV walls. More importantly, the majority (over 60%) of the ash particles entering the cooling chamber are trapped in the chamber for all four turbine inlet temperature conditions. This may reveal another volcanic ash damage mechanism originated in engine cooling flow passages, i.e., particle trap > geometry and heat transfer change > metal wall temperature increase > ash deposit and metal burn.

To develop the much-needed tools to mitigate and assess volcanic ash impact, some suggestions are recommended as follows:

(1) Define standard volcanic ash samples and study their physical, chemical and thermal properties for national and international partners;
(2) If possible, the cooling air used in engine miniature cooling passages should be filtered;
(3) Systematic analysis of engine airflow path-lines including the secondary air flows should be carried out, and identify potential problems;
(4) Carry out particle rebound and deposit tests on metal coupons at gas turbine relevant conditions, which will provide essential data to calibrate the developed numerical rebound and sticking models;
(5) Further improve the framework for practical engine design and fleet management, which can also be used to assess the aviation impact from other environmental particles.

Although to accurately qualitatively assess volcanic ash impact on gas turbines is a challenging field, with intelligent planning and collaboration, the dominating parameters can be identified, the required experimental tests can be cost-effectively carried out, and the much-needed tools can be built.

ACKNOWLEDGEMENTS

The authors are grateful to the Air Defence System Program, National Research Council of Canada for supporting this research project. The authors would also like to express their thanks to Dr. Ibrahim Yimer for the valuable comments and suggestions during the preparation of this manuscript.

REFERENCES

[1] NATO STO-AVT-213, RTG/Task Group 071, 2016, "Assessment of Volcanic Ash Effects on Military Platforms," Final Report of TR-AVT-213.

[2] Dunn, M.G., 2012, "Operation of Gas Turbine Engines in an Environment Contaminated With Volcanic Ash," Journal of Turbomachinery, Vol. 134 / 051001-1.

[3] Davison, C.R. and Rutke, T.A., 2014, "Assessment and Characterization of Volcanic Ash Threat to Gas Turbine Engine Performance," Journal of Engineering for Gas Turbines and Power, Vol. 136 / 081201-1.

[4] Mechnich, P., Braue, W. and Schulz, U., 2011, "High-Temperature Corrosion of EB-PVD Yttria Partially Stabilized Zirconia Thermal Barrier Coatings with an Artificial Volcanic Ash Overlay," Journal of American Ceramic Society, 94 [3], pp. 925–931.

[5] Song, W., Lavalle, Y., Hess, K.U, Kueppers, U., Cimarelli, C. and Dingwell, D.B., 2016, "Volcanic Ash Melting under Conditions Relevant to Ash Turbine Interactions," Nature Communications, DOI: 10.1038/ncomms10795.

[6] Kim, J., Dunn, M.G., Baran, A.J., Wade, D.P. and Tremba, E.L., 1993, "Deposition of Volcanic Materials in the Hot Sections of Two Gas Turbine Engines," Journal of Engineering for Gas Turbines and Power, 115, pp. 641-651.

[7] Padova, C., Dunn, M.G. and Moller, J.C., 1987, "Dust Phenomenology Testing in the Hot-section Simulator of an Allison T56 Gas Turbine," Calspan report No. 7389-A-1.

[8] Dunn, M.G., Padova, C., Moller, J.E. and Adams, R.E., 1987, "Performance Deterioration of a Turbofan and a Turbojet Engine upon Exposure to a Dust Environment," Journal of Engineering for Gas Turbines and Power, Vol. 109, pp. 336-343.

[9] Moller, J.C. and Dunn, M.G., 1989, "Dust and Smoke Phenomenology Testing in a Gas Turbine Hot Section Simulator," DNA-TR-90-72-V2.

[10] Kim, J., Baran, A.J. and Dunn, M.G., 1991, "Description of a F-100 Engine Hot Section Test System (HSTS) for Dust Phenomenology Testing,"DNA-TR-91-159.

[11] Kim, J., Dunn, M.G. and Baran, A.J., 1991, "The 'Most Probable' Dust Blend and its Response in the F-100 Hot Section Test System (HSTS)," DNA-TR-91-160.

[12] Jiang, L.Y., Wu, X. and Zhong Zhang, Z., 2014, "Conjugate Heat Transfer of an Internally Air-Cooled Nozzle Guide Vane and Shrouds," Advances in Mechanical Engineering, Article ID 146523, http://dx.doi.org/10.1155/2014/146523.

[13] Jiang, L.Y. and P. Andrew Corber, P.A., 2014, "Air Distribution over a Combustor Liner," IGTI paper, GT-2014-25405.

[14] Stiesch, G., 2003, "Modeling Engine Spray and Combustion Processes," Springer, New York.

[15] Fluent Inc., 2015, "Fluent 15 documentation," 10 Cavendish Court, Lebanon, NH 03766, USA.

[16] Jiang, L.Y., 2012, "A Critical Evaluation of Turbulence Modeling in a Model Combustor," ASME Turbo Expo, Copenhagen, Denmark, GT2012-68414.

[17] Kim, O.V. and Dunn, P.F., 2007, "A Microsphere-Surface Impact Model for Implementation in

Computational Fluid Dynamics," Aerosol Science, 38, pp. 532 – 549.

[18] Reagle, C.J., Delimont, J.M., Ng, W.F. and Ekkad, S.V., 2014, "Study of Micro-Particle Rebound Characteristics Under High Temperature Conditions," Journal of Engineering for Gas Turbines and Power, Vol. 136 / 011501-1.

[19] Ai, W. and Fletcher, T.H., 2009, "Computational Analysis of Conjugate Heat Transfer and Particulate Deposition on a High Pressure Turbine Vane," IGTI paper, GT2009-59573.

[20] El-Batsh, H. and Haselbacher, H., 2002, "Numerical Investigation of the Effect of Ash Particle Deposition on the Flow Field through Turbine Cascade," IGTI paper, GT-2002-30600.

[21] Brach, R. and Dunn, P., 1992, "A Mathematical Model of the Impact and Adhesion of Microspheres," Aerosol Science and Technology, Vol. 16, No. 1, pp. 51 - 64.

[22] Soltani, M. and Ahmadi, G., 1994, "On Particle Adhesion and Removal Mechanisms in Turbulent Flows," Journal of Adhesion Science Technology, Vol. 8, No. 7, pp. 763 – 785.

[23] Barker, B., Casaday, B., Shankara, P., Ameri, A. and Bons, J.P., 2013, "Coal Ash Deposition on Nozzle Guide Vanes—Part II: Computational Modelling," Journal of Turbomachinery, Vol. 135 / 011015-1.

[24] Tafti, D. K. and Sreedharan, S. S., 2010, "Composition Dependent Model for the Prediction of Syngas Ash Deposition with Application to a Leading Edge Turbine Vane," IGTI paper, GT2010-23655.

[25] Prenter, R., Whitaker, S.M., Ameri, A., Bons, J.P., 2014, "The Effects of Slot Film Cooling on Deposition on a Nozzle Guide Vane," AGTI paper, GT2014-27171.

[26] N'dala, I., Cambier, F., Anseau, M. R. and Urbain, G., 1984, "Viscosity of Liquid Feldspars. Part I: Viscosity Measurements," Transactions & Journal of the British Ceramic Society, Vol. 83, pp. 108–112.

[27] Ebert, H.P, Hemberger, F., Fricke, J., Büttner, R. Bez, S. and Zimanowski, B., 2002, "Thermo-Physical Properties of a Volcanic Rock Material," High Temperatures - High Pressures, volume 34, pp. 561 – 568.

[28] Lekki, J. et al, 2013, "Status Report," Multi-Partner Experiment to Test Volcanic-Ash Ingestion by a Jet Engine.

[29] Giordano, D., Russell, J.R. and Dingwell, D.B., 2008, "Viscosity of Magmatic Liquids: A Model," Earth and Planetary Science Letters 271, pp. 123–134.

[30] Riley, C.M., Rose, W.I. and Bluth, G.J.S., 2003, "Quantitative Shape Measurements of Distal Volcanic Ash," Journal of Geophysical Research, Vol. 108, NO. B10, 2504, doi:10.1029/2001JB000818.

[31] De Giorgi, M.G., Campilongo, S. and Ficarella, A., 2013, "Experimental and Numerical Study of Particle Ingestion in Aircraft Engine," IGTI paper, GT2013-95662.

[32] https://en.wikipedia.org/wiki/Volcanic_ash.

[33] Oechsle, V.L., Ross, P.T. and Mongia, H.C., 1987, "High Density Fuel Effects on Gas Turbine Engines," AIAA-87-1829, San Diego California, USA, AIAA/SAE/ASME/ASEE 23rd Joint Propulsion Conference.

[34] Jiang, L.Y. and Corber, A., 2011, "Benchmark Modeling of T56 Gas Turbine Combustor --- Phase I, CFD Model, Flow Features, Air Distribution and Combustor Can Temperature Distribution," LTR-GTL-2010-0088, Aerospace, National Research Council Canada.

[35] Rizk, N.K., Oechsle, V.L., Ross, P.T., and Mongia, H.C., 1988, "High Density Fuel Effects," Technical Report AFWAL-TR-88-2046, Wright-Patterson Air Force Base, Aero Propulsion Laboratory.

[36] Clarkson, R. (Rolls-Royce), 2015, "Volcanic Ash and Gas Turbine Aero Engines – Update," WMO VAAC Best Practice Workshop, May 5th- 8th.

[37] Lekki, J., Lyall, E., Guffanti, M., Fisher, J., Erlund, B., Clarkson, R. and van de Wall, A., 2013, "Multi-Partner Experiment to Test Volcanic-Ash Ingestion by a Jet Engine, Status Report."